BILINGUAL PUBLISHING GROUP

Advances in Geological and Geotechnical Engineering Research

https://journals.bilpubgroup.com/index.php/agger

ARTICLE

Amplitude Variation with Offset (AVO) Inversion for Reservoir Visualization: A Case Study of Taje Field, Niger Delta, Nigeria

Ebiegberi Oborie [*], ***Omonefe Francis***, ***Desmond Eteh***

Department of Geology, Niger Delta University, Bayelsa State, 560103, Nigeria

ABSTRACT

Amplitude Variation with Offset (AVO) inversion analysis was performed on pre-stack seismic data and well information gathered from the shallow offshore area of the Niger Delta. This analysis aimed to improve reservoir visualization and employed the Hampson Russell Geoview, AVO, and STRATA software tools. The seismic data were provided in Seg-Y format, covering an in-line range from 4503 to 5569, an x line range from 1434 to 2026, and an angle of incidence range of 0 to 45°. The study centered on the Taje well_026. Within the subsurface, the authors identified five distinct reservoirs, labeled A to E, located at various depths ranging from 3057.50 to 3115.00 m, 3115.00 to 3157.50 m, 3157.50 to 3190.00 m, 3190.00 to 3200.00 m, and 3200.00 to 3239.00 m, respectively. These reservoirs exhibited different fluid compositions. Reservoir A, primarily composed of sandstone, contained brine, whereas Reservoirs B and D, dominated by shale, contained gas. On the other hand, Reservoirs C and E, both comprised of sandstone, held oil. Reservoir C is distinguished by its clean sandstone unit. The inversion results revealed that both Reservoirs C and E consisted of low impedance sand layers surrounded by higher impedance shale layers. The gas migrated from the reservoir and was trapped within the shale units due to deformation of the lithological units, likely induced by stress accumulation. This migration process was facilitated by the shale's inability to undergo smearing, possibly as a result of faulting mechanisms.

Keywords: Taje; Seismic inversion; AVO; Prestack; Niger Delta

1. Introduction

In exploration seismology, seismic reflection is employed to locate potential hydrocarbon traps [1]. However, the absence of hydrocarbons in these traps poses a significant risk. Scientists have sought better methods to identify hydrocarbons on seismic

*CORRESPONDING AUTHOR:
Ebiegberi Oborie, Department of Geology, Niger Delta University, Bayelsa State, 560103, Nigeria; Email: geosoftconsultingltd@gmail.com

ARTICLE INFO
Received: 14 December 2023 | Revised: 30 January 2024 | Accepted: 18 February 2024 | Published Online: 29 February 2024
DOI: https://doi.org/10.30564/agger.v6i1.6158

CITATION
Oborie, E., Francis, O., Eteh, D., 2024. Amplitude Variation with Offset (AVO) Inversion for Reservoir Visualization: A Case Study of Taje Field, Niger Delta, Nigeria. Advances in Geological and Geotechnical Engineering Research. 6(1): 21–32. DOI: https://doi.org/10.30564/agger.v6i1.6158

sections, with the hope of enhancing exploratory seismology [2]. Bright spots, characterized by reflections with high amplitudes, have been occasionally associated with gas presence [3].

To identify gas directly on seismic recordings, a more reliable indicator than bright spots on stacked sections is required [4]. Li (2021) demonstrated that gas-sand reflection coefficients exhibit unique behavior with increasing offset, serving as a direct hydrocarbon indicator on seismic data [5]. This discovery prompted seismic interpreters to focus on quantitative techniques, such as AVO analysis, acoustic and elastic impedance inversion, forward seismic modeling, and post-stack amplitude analysis, which can provide valuable information beyond conventional seismic interpretation. Seismic reflectivity inversion and interpretation have heavily relied on Acoustic Impedance (AI) since its introduction in the 1970s. AI is valued for its strong agreement with rock attributes measured in experiments and field data [6]. Unlike seismic reflectivity, which occurs at the interfaces of different strata, AI values remain constant within rock layers, simplifying the link with geology and stratigraphy. Inversion is commonly used to extract impedance from seismic reflection data [7].

Seismic inversion involves building an earth model consistent with observed seismic data, aiming to convert seismic reflection spikes at geological boundaries into relevant mechanical layer parameters (impedances) [8,9,2]. However, seismic inversion is non-unique and computationally intensive [10]. The Monte Carlo method has been used to address non-uniqueness by generating numerous initial models [11]. Inversion converts reflection amplitudes into Acoustic Impedance (AI), where $AI = V_P\rho$, with V_P representing P-wave velocity and ρ representing density. Impedance logs obtained from well data can be directly compared to seismic AI, facilitating lithological and stratigraphic interpretation [12]. AI transformations are crucial for seismic interpretation and reservoir characterization, particularly in identifying fluid-filled and porous zones [9]. Typically, stacked seismic data are used to estimate normal-incidence reflectivity, from which AI is inverted [6].

According to Zhou et al. (2022) [13], Ostrander was the first to highlight the potential of gas-sand reflection coefficients as hydrocarbon indicators at increasing offsets, therefore, the Amplitude Variation with Offset (AVO) technique, to assess reservoir fluid capacity, was developed. AVO models were created and compared to common-offset stacks from actual seismic data [14]. According to Russell et al. (2001) [15], Aki and Richards' equation for seismic reflectivity with the mudrock line was first integrated to highlight anomalies indicating hydrocarbon reserves. Today, AVO analysis and seismic inversion are routinely used to derive seismic features indicative of hydrocarbons, including acoustic impedance (AI), shear impedance (Z_S), elastic impedance (EI), Lamé parameters (LMR), and the V_P/V_S ratio. These properties help characterize rock matrix, pore fluid, and reflectivities, which can be extracted from seismic traces and combined with observed velocities to compute density [16]. Pre-stack (AVO) inversion employs fluctuations in reflection amplitudes within Common Midpoint Gathers (CMP) to determine elastic properties (V_P, V_S, ρ) and infer petrophysical properties and fluid/gas saturation [12]. Both post-stack and pre-stack seismic data benefit from amplitude fluctuations and play a significant role in hydrocarbon exploration, particularly in gas reserves [17].

In recent days, AVO analysis has been widely applied in hydrocarbon exploration studies [18–22]. In the Niger Delta, AVO techniques have been used to determine anomalous and gas zones in wells [23–27], detect hydrocarbon reservoirs on pre-stack time seismic data [28], and identify hydrocarbon-charged reservoirs using Rock physics modeling and Lamda-Mu-Rho (LMR) seismic inversion [28]. The focus of the research has primarily been on conducting AVO Inversion analysis on pre-stack seismic data and well information to reveal geologic structures and impedance contrasts within lithology.

2. Geological settings

The study area is an Oil field located within the offshores of Niger Delta. It is located at Long. 6.5–7.5 and Lat. 4.219–4.6 (**Figure 1**). The Niger Delta Basin, which potentially provides access to Camer-

oon, Equatorial Guinea, and São Tomé and Príncipe, is an extensional rift basin [29]. This basin is located along Nigeria's western coast within the passive continental margin between the Niger Delta and the Gulf of Guinea. It holds immense economic significance due to its extensive petroleum infrastructure [30]. The Niger Delta is one of Africa's largest subaerial basins, covering a total area of 300,000 km^2 with a sediment fill of 500,000 km^3 and a subaerial extent of approximately 75,000 km^2 (**Figure 1**). The sediment fill is remarkably deep, ranging from nine to twelve kilometers. Within this basin, a diverse range of geological formations provides valuable insights into local, regional, and global tectonics, as well as the basin's formation history.

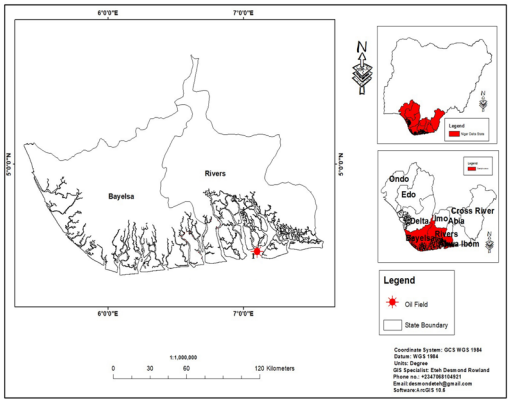

Figure 1. Map of Niger Delta showing study area.

The Niger Delta Basin is part of the broader geological structure known as the Benue Trough, situated in its southernmost segment. On the opposite side of the basin, it is defined by the Cameroon Volcanic Line and the transform passive continental margin [28]. The Niger Delta is globally recognized as the tenth-largest province for oil and gas resources. It currently yields slightly over 2 million barrels of oil daily [31]. The estimated reserves in this region are substantial, with projections indicating approximately 34.5 billion barrels of oil and 94 trillion cubic feet of natural gas. Oil companies continue to conduct extensive exploration activities in this area, making it one of the world's major oil producers [32]. The formation of the Niger Delta Basin is attributed to the separation of the South American plate from the African plate during the expansion of the South Atlantic. This separation resulted in a failed rift junction, leading to the creation of the Niger Delta Basin. The rifting process occurred from the late Jurassic to the middle Cretaceous and gave rise to numerous faults, including many thrust faults [33]. During the late Cretaceous, syn-rift sands and later shales were deposited, suggesting a gradual coastline retreat during this period [32] (**Figure 2**). Concurrently, the basin continued to expand, resulting in high-angle normal faults and fault block rotations. The Paleocene marked a significant coastline transgression in the basin's history. The Niger Delta Basin comprises three primary formations: the Benin, Agbada, and Akata formations. The Akata Formation was formed during the Paleocene, while the Agbada Formation originated during the Eocene. Loading from overlying sediments caused the underlying shale Akata Formation to form shale diapirs. The Benin Formation was subsequently deposited during the Oligocene and continues to accumulate to this day. Due to the basin's geological complexity, it is divided into distinct zones [29] as illustrated in **Figure 2** The presence of a thicker crust has resulted in an extensional zone on the continental shelf. In the deep-sea part of the basin, there are transition and contraction zones that move basinward [30].

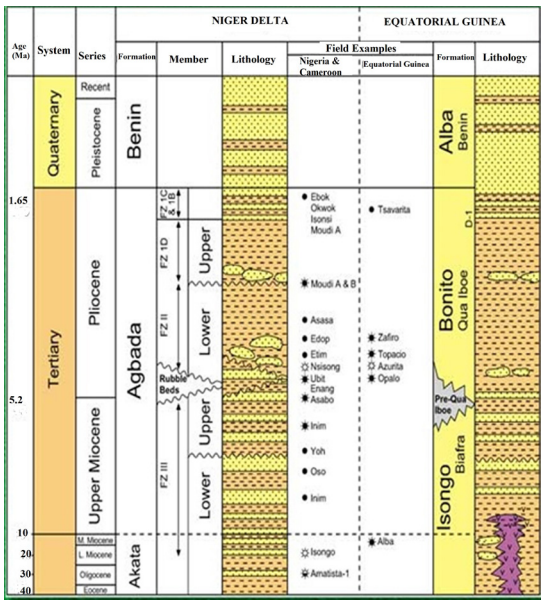

Figure 2. Section stratigraphy of the Niger Delta Basin.

Source: Ogbe, O.B. [30].

3. Materials and methods

The data used in this analysis originates from the "Taje" oil field in the Niger Delta, South-South Nigeria. The data have undergone migration and a comprehensive Amplitude Variation with Offset (AVO) process before stacking. The analysis relies on both well data and a 3D pre-stack seismic volume. The Hampson-Russell software (HR10.0.3) was employed for this work. This software, developed by Dan Hampson and Brian Russell in 1987, is renowned for its safety and effectiveness in conducting AVO modeling, inversion, processing, and analyses, utilizing well log and seismic data as initial information.

The typical workflow for either post-stack or pre-stack inversion consists of the following steps:

1) Start GeoView.
2) Load wells into GeoView.
3) Start STRATA.
4) Load seismic data into STRATA.
5) Load and display the horizon map.
6) Correlate each well with the seismic volume and extract one or more wavelets.
7) Build an initial model for inversion.
8) Run inversion analysis
9) Run inversion over the volume and analyze the results.

Post-stack seismic volume was not available for this work to help create an acoustic impedance volume. To preserve the set objectives, the desired impedance volume was created from pre-stack seismic inversion alongside other volumes. Order than being able to create other impedance volumes, a step unattainable by post-stack inversion, the pre-stack seismic inversion method also has the potential of revealing subsurface geologic structures and reservoir properties used to analyze the fluid content of a sand reservoir. Lamda-Mu-Rho (LMR) inversion was performed as a pre-stack analysis.

The objective of the pre-stack seismic inversion process was to obtain reliable estimates of P-wave velocity (V_P), S-wave velocity (V_S), and density (ρ) and use them to predict the fluid and lithology properties of the sand reservoir which occur around 3100 ms.

In this study, the horizons were picked manually close to and within the zone of interest. Two statistical wavelets were extracted from a near angle of 0 to 15° and a far angle of 15 to 30° respectively for the inversion process. This was done because pre-stack inversion requires a wavelet that varies with angle. A time ranging from 700 to 5300 ms and an offset ranging from 3100 to 5300 ms was also used. The s-wave velocity, p-wave velocity, and density logs were used as typical setup parameters to create the initial model for pre-stack inversion.

Pre-stack inversion analysis is the process of applying the inversion at the well locations to verify the inversion parameters and optimize the seismic scaling. This was performed before the inversion of the entire volume by using angle gather as an input volume, the angle range of 0 to 45 found in the trace header, a number of the model parameters and the midpoint of the angle range of the two extracted wavelets as input parameters. Plots of In(Z_s) vs In(Z_p) and In(Density) vs In(Zp) were automatically displayed in the good data cross plot window. These plots when interpreted have the potential of revealing the presence or absence of hydrocarbon.

The inversion analysis results are displayed by specifying which amongst the Z_p, Z_s and density models to be inverted, how the inversion trace scaler will be calculated and which log curves will be plotted. The workflow for pre-stack inversion parameters is shown in **Figure 3a**.

In addition, an independent inversion for P and S-impedance was performed following the workflow depicted in **Figure 3b**. This approach is termed "independent" inversion because it initiates by extracting separate estimates of zero-offset P and S reflectivities from the seismic gathers. This is done using the Fatti equation which is given as:

$$R_{PP}(\theta) = c_1 R_{P0} + c_2 R_{S0} + c_3 R_D \tag{1}$$

where $c_1 = 1 + tan^2\,\theta$, $c_2 = \frac{-8\,sin^2\,\theta}{\gamma_{sat}^2}$, $c_3 = \frac{1}{2}tan^2\,\theta - \frac{2\,sin^2\,\theta}{\gamma_{sat}^2}$, $R_{S0} = \frac{1}{2}\left[\frac{\Delta V_S}{V_S} + \frac{\Delta\rho}{\rho}\right]$, and $R_D = \frac{\Delta\rho}{\rho}$.

The third term from the above Fatti equation

which consists of c_3R_D is dropped when considering how to extract R_P and R_S from an N-trace gather.

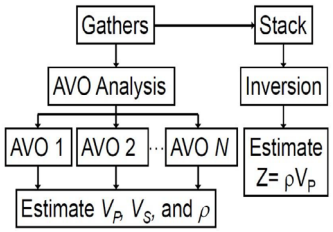

Figure 3a. Work flow for seismic lithology and fluid estimation using the AVO method.

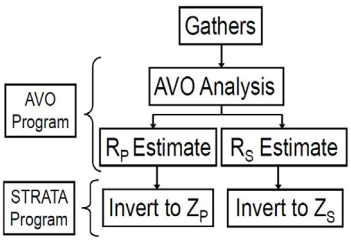

Figure 3b. Work flow for independent inversion for P and S-impedance.

4. Results and discussion

The results of this study are presented in many sections described below:

4.1 Petrophysical evaluation

Five reservoir units labeled A, B, C, D, and E, were identified at depths ranging from 3057.50–3115.00 m, 3115.00–3157.50 m, 3157.50–3190.00 m, 3190.00–3200.00 m and 3200.00–3239.00 m respectively (**Figure 4**). The units occurred in a paralic sequence of sandstone and shale following the alphabetical order. Of the five reservoirs, four (B, C, D, and E) were saturated with hydrocarbon fluid. Reservoir C consists of a clean sandstone unit with very prominent AVO anomalies. This unit was delineated with tops and a red marker. Parameters for this zone were extracted and used for the AVO study. The sandstone units (labeled A, C, and E) were observed to be competent, while the shale units (B and D) were observed to consist of soft shale. The shale served as a seal and source rock to our reservoir of interest respectively. Three fluid types (i.e., brine, gas, and oil) saturated the different units. The first unit (A) is saturated with brine; B and D are saturated with gas, while oil exists within reservoirs C and E respectively. The shale units have low permeability which greatly inhibits the gas from migrating to more permeable reservoir rocks. Thus, horizontal drilling was employed to produce shale gas since the gas would not flow from the formation at high rates.

Five different fluid contacts were also identified at depths of 3057.50 m, 3115.00 m, 3157.50 m, 3190.00 m, and 3200 m respectively. This includes the gas-water contact (gwc), water-gas contact (wgc), gas-oil contact (goc), oil-gas contact (ogc) and gas-oil contact (goc). The porosity and water saturation values for the reservoirs are presented in **Table 1**. The result further showed that Taje well_026 is an oil and gas field with high brine saturation.

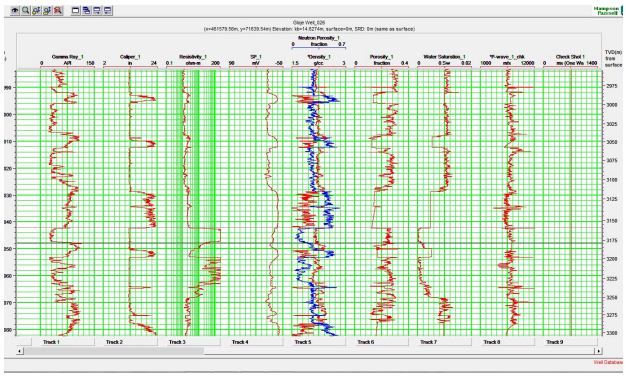

Figure 4. Results of well log analysis of Taje well_026.

Table 1. Summary of results of well log analysis of Taje well_026.

Reservoir Unit	Depth (m)		Thickness (m)	Porosity Fraction	Water Saturation%	Lithology	Fluid Type
	Top	Base					
A	3057.50	3115.00	57.50	0.23	0.71	Sandstone	Brine
B	3115.00	3157.50	42.50	0.05	0.14	Shale	Gas
C	3157.50	3190.00	32.50	0.12	0.22	Clean sandstone	Oil
D	3190.00	3200.00	10.00	0.07	0.11	Shale	Gas
E	3200.00	3239.00	39.00	0.17	0.20	Sandstone	Oil

4.2 AVO inversion

Using pre-stack inversion analysis, the inversion parameters are checked and the seismic scaling is optimized at well sites. This was performed before the inversion of the entire volume by using angle gather as an input volume, the angle range of 0 to 45 found in the trace header, a number of the model parameters, and the midpoint of the angle range of the two extracted wavelets as input parameters (**Figure 5**). A fluid replacement modeling was performed to calculate the correct S-wave behaviour for the gas sand. Within the clean sandstone reservoir section (unit C), it was observed that the amplitude of the density log and that of Poisson's ratio log decreased, the P-wave log increased slightly, while the S-wave log increased. However, the non-hydrocarbon sands, outside the bright spot (unit B), show relatively low amplitudes. Values for the estimated rock elastic parameter are presented in **Table 2**. The result shows a low acoustic impedance value of 6201.16 Pa·s/m^3 for reservoir C compared to that of the bounding shale lithology which has a higher value of 6598.93 Pa·s/m^3.

To display the initial model, only an impedance volume with a coloured strip at each CDP location was displayed (**Figure 6**). The colour strips at each CDP location represent the impedance. The default display did not show the model in a continuous form because the input seismic data was pre-stack. The complete models in colour were displayed by temporarily turning off the seismic traces.

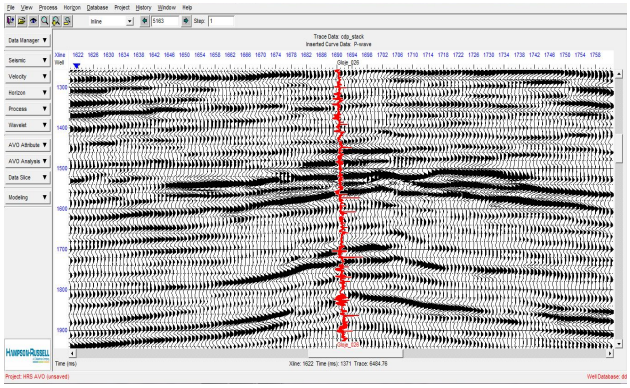

Figure 5. Result of processed CDP stack.

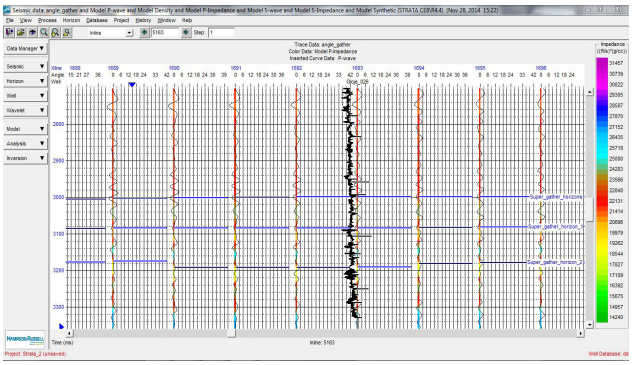

Figure 6. Initial model for pre-stack inversion.

Table 2. Values for the estimated rock elastic parameter.

Reservoir	Lithology	Depth (m)	V_P (m/s)	V_s (m/s)	ρ (g/cc)	Z_P Pa·s/m^3
A	Sandstone	3057.50	3207.17	1592.26	1.796	5760.08
B	Shale	3115.00	3462.19	1812.06	1.906	6598.93
C	Sandstone	3157.50	3108.35	1802.36	1.995	6201.16
D	Shale	3190.00	3261.56	1479.86	1.894	6177.39
E	Sandstone	3200.00	3315.36	1676.44	2.139	7091.56

The low-frequency initial model results of Z_P, Z_S, density, and synthetic displayed in colour plots are shown in **Figures 7a–7d** respectively. The results reflect a faulted anticlinal structural trap with very good impedance contrasts. Also observed was a low impedance colour displayed along the zone of interest (clean sandstone reservoir unit) bounded by higher colour impedance shale units. The reservoir units labeled A, B, C, D, and E in the model results correspond to those identified in **Table 2**.

Using the angle gathered as the input volume, the midpoints of the angle range of the extracted near (i.e., 7.5°, from 0–15°) and far (i.e., 22.5°, from 15–30°) statistical wavelets, were extracted and used to create a new wavelet (see **Figures 8a and 8b**).

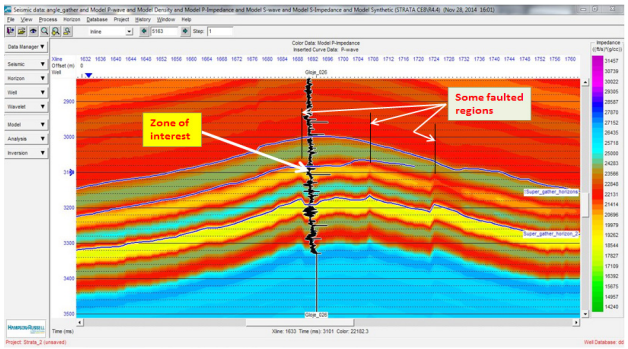

Figure 7a. Result of P-impedance (Z_P) model.

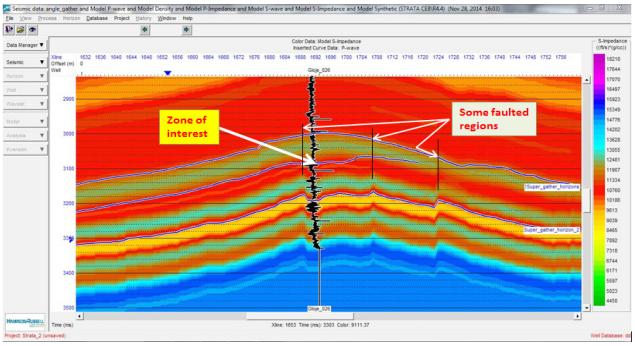

Figure 7b. Result of S-impedance (Z_S) model.

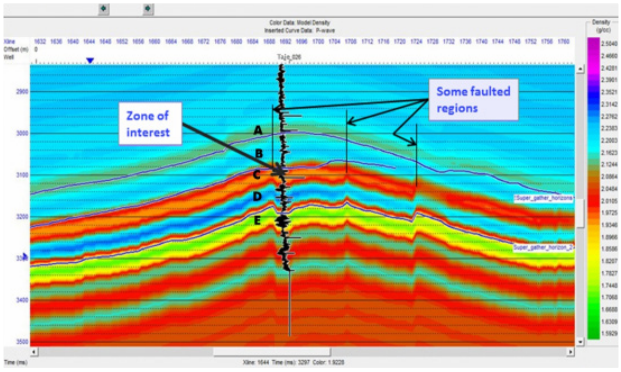

Figure 7c. Result of density model.

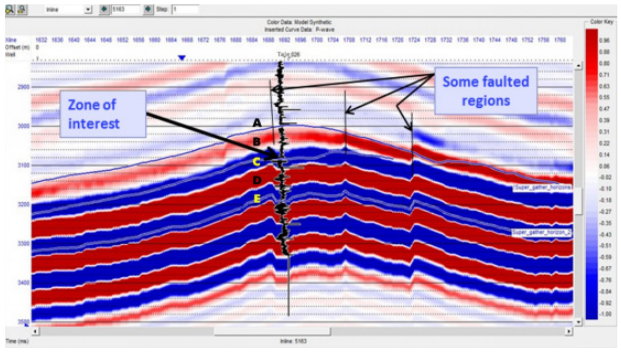

Figure 7d. Result of the synthetic model.

The displayed cross plot of $\ln(Z_S)$ vs $\ln(Z_P)$ and $\ln(\rho)$ vs $\ln(Z_P)$ in **Figure 9a** was used to set the relationship between $\ln(Z_p)$, $\ln(Z_s)$, and ln(Density). The regression fit was manually fitted through the clusters to obtain an improved estimate as shown in **Figure 9b**. This was done to discriminate possible fluid saturated zones. The cluster points which fall away from the trend line show the presence of hydrocarbon anomalies (Russell and Hampson 2006). These points were delineated by two red ellipses and tagged $\Delta In(Z_s)$ and $\Delta In(\rho)$ respectively.

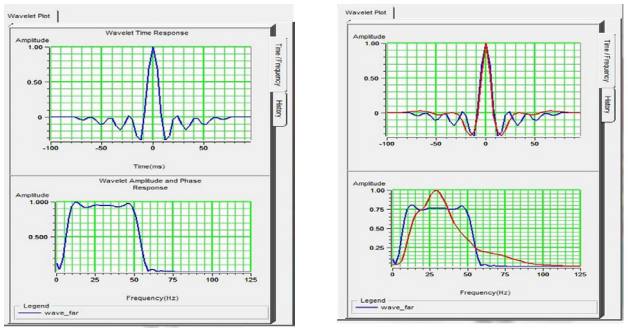

Figure 8. Wavelet for pre-stack analysis. (a) Before making modifications. (b) After making modifications.

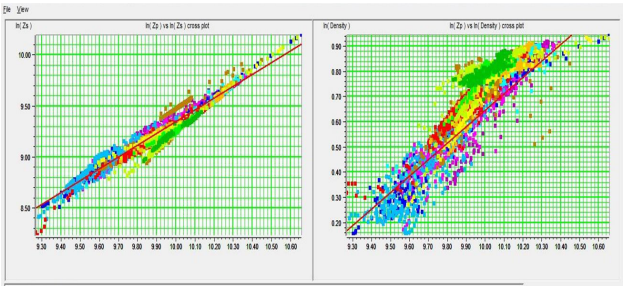

Figure 9a. Regression coefficients were calculated for P-impedance (Z_p), S-impedance (Z_s) and density (ρ), (before making modifications).

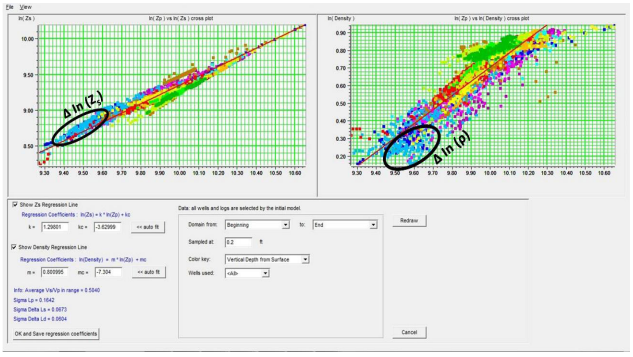

Figure 9b. Regression coefficients calculated for P-impedance (Z_p), S-impedance (Z_s) and density (ρ), show a good fit with the regression lines.

The inversion analysis result is displayed in log curves (**Figure 10a**). The display shows several useful curves before making modifications. These include the synthetic, the real data, and the error. **Figure 10b** shows the result of **Figure 9b** after making modifications. Results of **Figure 10b** show the curves inverted for P-impedance (Z_P), S-impedance (Z_S), and V_P/V_S ratio and their comparison with the real traces. As shown in the result, each set of curves displayed in the left panel shows an overlay of three impedance curves: the original impedance log (real log) in blue, the initial guess model in black, and the final inverted curve result in red. The inverted curves show a very good correlation with the original impedance curves.

The synthetic traces calculated from the inversion results (see the second panel of **Figure 10b**) show a very good correlation value of 99.8% when compared with the input seismic trace. A practically zero error value (0.063) obtained by finding the difference between the synthetic and the input seismic trace (see the third panel of **Figure 10b**) indicates that the inversion has created an acoustic impedance trace consistent with the wavelet and the input seismic trace. The results of the inversion parameter were applied and used to create the inverted volumes. These volumes include the inverted Z_P volume (**Figure 11a**), the inverted Z_S volume (**Figure 11b**), the density volume (**Figure 11c**), and the inverted V_P/V_S volume (**Figure 11d**).

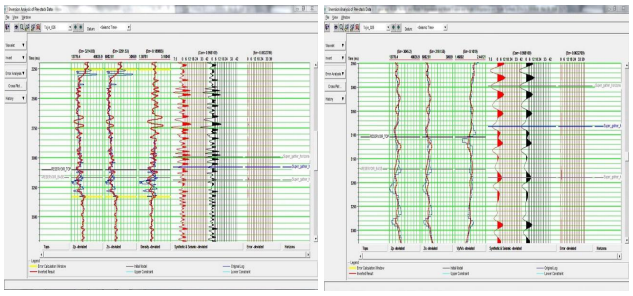

Figure 10. Inversion result at the location of Taje well_026. (a) Before making some modifications. (b) After making some modifications.

The inverted angle gathers volume was created to generate the residual error volume by subtracting it from the input angle gather. The result shows a practically zero error value of 0.063. This indicates that the inversion has created an acoustic impedance trace consistent with the wavelet and the input seismic trace. There was a drop in impedance in the gas sand zone for inverted volumes of P-impedance (**Figure 11a**), density impedance (**Figure 11c**) and V_P/V_S ratio (**Figure 11d**) but increases for the S-impedance (**Figure 11b**).

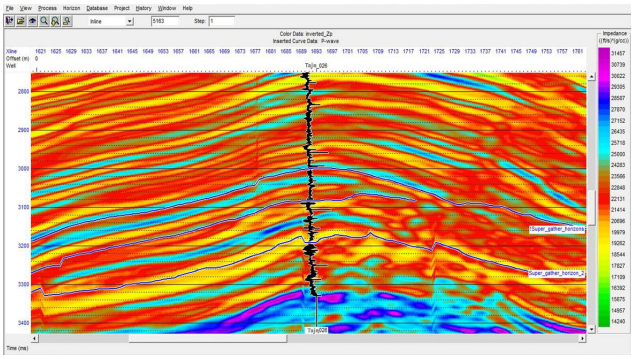

Figure 11a. Result of inverted Z_p volume.

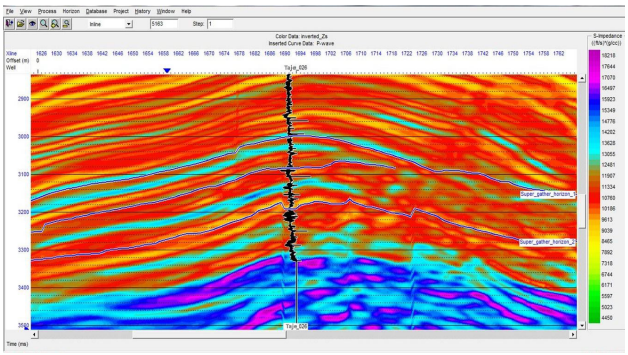

Figure 11b. Result of inverted Z_S volume.

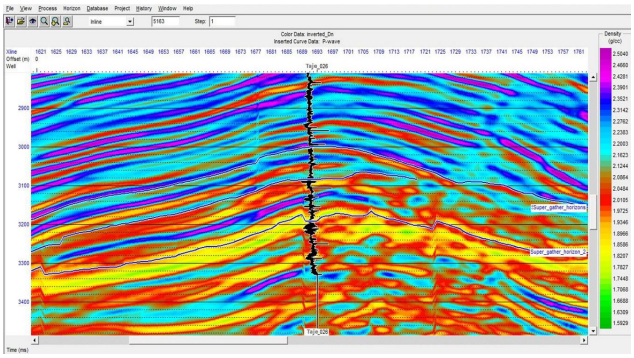

Figure 11c. Result of inverted density volume.

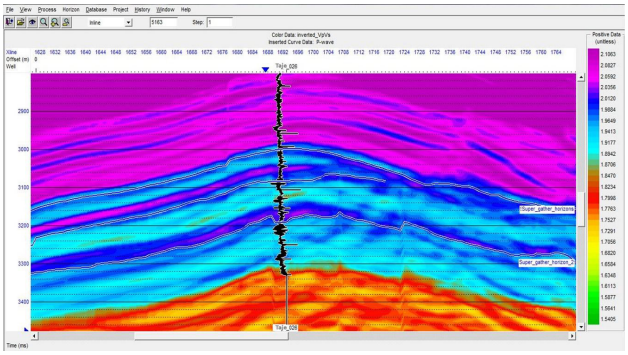

Figure 11d. Result of inverted Vp/Vs volume.

Therefore, the inverted impedance volume results also show a pictorial view of the geologic structures, the stratigraphic units, and the fluid emplacement in terms of impedance contrasts. These were prominent in all the volumes. Anticline and faults are the two observed structures. They combine to form a faulted anticlinal structure and serve as structural traps for the hydrocarbon fluids. The stratigraphic unit revealed consists of a paralic sequence of sandstone and shale. Oil was observed within the sandstone units (reservoirs), while the gas deposits that were observed in the shale units, escaped from the reservoir (sandstone units) through the fault planes. The shales were observed to occur in thin lenses and as such could not smear to serve as a seal after fracturing. The impedance at the reservoir units was observed to be acoustically lower than those of the bounding lithologies. The AVO inversion results revealed that both Reservoirs C and E consisted of low impedance sand layers surrounded by higher impedance shale layers. Importantly, the study found that gas migrated from Reservoirs B and D (shale-dominated) and became trapped within the shale units. This gas trapping phenomenon was attributed to the deformation of lithological units, which was likely induced by stress accumulation.

The migration process of gas from the reservoirs was facilitated by the shale's inability to undergo smearing, possibly due to faulting mechanisms. Faulting can create pathways for fluid migration and alter the mechanical properties of the shale, leading to deformation. In this context, stress accumulation within the subsurface could induce deformation in the shale units, creating pathways for gas migration. The inability of shale to undergo smearing implies that the gas, once migrated, remains trapped within the shale layers, forming potential gas reservoirs.

5. Conclusions

In conclusion, the Amplitude Variation with Offset (AVO) inversion analysis conducted on pre-stack seismic data from the shallow offshore area of the Niger Delta has made significant contributions to our understanding of the subsurface reservoirs in the Taje well_026 region. The study employed advanced software tools, including Hampson Russell Geoview, AVO, and STRATA, to enhance reservoir visualization and interpretation.

The analysis identified five distinct reservoirs (A to E) at varying depths, each exhibiting unique fluid compositions. Reservoir A, predominantly sandstone, contained brine, while Reservoirs B and D, dominated by shale, held gas. Reservoirs C and E, composed of sandstone, contained oil, with Reservoir C distinguished by its clean sandstone unit.

The inversion results reveal that both Reservoirs C and E consisted of low impedance sand layers surrounded by higher impedance shale layers. The migration of gas from these reservoirs and its subsequent trapping within shale units were attributed to the deformation of lithological units, likely induced by stress accumulation. The study suggests that this migration process was facilitated by the shale's inability to undergo smearing, possibly as a result of faulting mechanisms.

Overall, this research not only enhances our knowledge of the geological and fluid composition of the subsurface reservoirs in the Niger Delta but also contributes to the understanding of the migration and trapping mechanisms of hydrocarbons. These findings have practical implications for the oil and gas industry, providing valuable information for reservoir characterization and exploration strategies in similar geological settings. The integration of AVO inversion analysis with good information and seismic data proves to be a powerful tool for improving reservoir characterization and understanding

the complex dynamics of hydrocarbon reservoirs in offshore environments.

Author Contributions

O.E. developed the study with part of the writing and Formatting, O.F. processed the data and E.D. assisted with writing. The final version was co-written by all authors.

Conflict of Interest

There is no conflict of interest.

Funding

This research received no external funding.

References

[1] Oumarou, S., Mabrouk, D., Tabod, T.C., et al., 2021. Seismic attributes in reservoir characterization: An overview. Arabian Journal of Geosciences. 14, 402.

[2] Farfour, M., El-Ghali, M.A., Gaci, S., et al., 2021. Seismic attributes for hydrocarbon detection and reservoir characterization: A case study from Poseidon field, Northwestern Australia. Arabian Journal of Geosciences. 14, 2814.
DOI: https://doi.org/10.1007/s12517-021-08853-y

[3] Ilozobhie, A.J., Egu, D.I., 2021. Dynamic reservoir sand characterization of an oil field in the Niger Delta from seismic and well log data. Arabian Journal of Geosciences. 14, 853.
DOI: https://doi.org/10.1007/s12517-021-06542-4

[4] Etuk, N.O., Aka, M.U., Agbasi, O.E., et al., 2020. Evaluation of seismic attributes for reservoircharacterization over Edi field, Niger delta, Nigeria using 3d seismic data. International Journal of Advanced Geosciences. 8(2).
DOI: https://doi.org/10.14419/ijag.v8i2.31043

[5] Li, J., 2021. Vibration response test method of curtain wall under seismic coupling. Arabian Journal of Geosciences. 14, 468.
DOI: https://doi.org/10.1007/s12517-021-06849-2

[6] Chen, H., Sacchi, M.D., Haghshenas Lari, H., et al., 2023. Nonstationary seismic reflectivity inversion based on prior-engaged semisupervised deep learning method. Geophysics. 88(1), WA115–WA128.
DOI: https://doi.org/10.1190/geo2022-0057.1

[7] Li, C., Liu, X., 2022. Sparse seismic reflectivity inversion using an adaptive fast iterative shrinkage-thresholding algorithm. Geophysical Prospecting. 70(6), 1003–1015.
DOI: https://doi.org/10.1111/1365-2478.13211

[8] Luo, C., Ba, J., Carcione, J.M., et al., 2020. Joint PP and PS pre-stack seismic inversion for stratified models based on the propagator matrix forward engine. Surveys in Geophysics. 41, 987–1028.
DOI: https://doi.org/10.1007/s10712-020-09605-5

[9] Xiao, S., Ba, J., Guo, Q., et al., 2020. Seismic pre-stack AVA inversion scheme based on lithology constraints. Journal of Geophysics and Engineering. 17(3), 411–428.
DOI: https://doi.org/10.1093/jge/gxaa001

[10] Luo, C., Li, X., Huang, G., 2019. Pre-stack AVA inversion by using propagator matrix forward modeling. Pure and Applied Geophysics. 176, 4445–4476.
DOI: https://doi.org/10.1007/s00024-019-02157-9

[11] Luengo, D., Martino, L., Bugallo, M., et al., 2020. A survey of Monte Carlo methods for parameter estimation. EURASIP Journal on Advances in Signal Processing. (1), 25.
DOI: https://doi.org/10.1186/s13634-020-00675-6

[12] Omonefe, F., Ejaita, E., 2020. AVO fluid inversion (AFI) technique as a tool to predict reservoir fluid content using data from FD field, onshore Niger Delta Nigeria. International Journal of Creative and Innovative Research in All Studies. 3(2).

[13] Zhou, D., Wen, X., He, X., et al., 2022. Second-order approximate expressions of P-and SV-plane-wave reflection coefficients at the solid/solid media interface. Geophysics. 87(5), N85–N94.
DOI: https://doi.org/10.1190/geo2021-0627.1

[14] Russell, B.H., Gray, D., Hampson, D.P., 2011. Linearized AVO and poroelasticity. Geophysics. 76(3), C19–C29.
DOI: https://doi.org/10.1190/1.3555082

[15] Russell, B.H., Lines, L.R., Hirsche, K.W., et al., 2001. The AVO modelling volume. Exploration Geophysics. 32(4), 264–270.
DOI: https://doi.org/10.1071/EG01264

[16] Durrani, M.Z.A., Rahman, S.A., Talib, M., et al., 2023. Discrimination of lithofacies in tight gas reservoir using field-specific rock physics modeling scheme. A case study from a mature field of middle Indus Basin, Pakistan. Acta Geophysica. 71, 2763–2780.
DOI: https://doi.org/10.1007/s11600-023-01069-6

[17] Francis, O., Oborie, E., 2022. History and reviews on amplitude variation with offset (AVO) technology. International Journal of Advances in Engineering and Management (IJAEM). 4(6), 2437–2449.

[18] Kumar, D., Zhao, Z., Foster, D.J., et al., 2020. Frequency-dependent AVO analysis using the scattering response of a layered reservoir. Geophysics. 85(2), N1–N16.
DOI: https://doi.org/10.1190/geo2019-0167.1

[19] Zhao, Z., Kumar, D., Foster, D.J., et al., 2021. Frequency-dependent AVO analysis: A potential seismic attribute for thin-bed identification. Geophysics. 86(4), N1–N17.
DOI: https://doi.org/10.1190/geo2020-0777.1

[20] Skopintseva, L., Aizenberg, A., Ayzenberg, M., et al., 2012. The effect of interface curvature on AVO inversion of near-critical and postcritical PP-reflections. Geophysics. 77(5), N1–N16.
DOI: https://doi.org/10.1190/geo2011-0298.1

[21] Santoso, D., Kadir, W.G.A., Alawiyah, S., 2000. Delineation of reservoir boundary using AVO analysis. Exploration Geophysics. 31(1–2), 409–412.
DOI: https://doi.org/10.1071/eg00409

[22] Beretta, M.M., Bernasconi, G., Drufuca, G., 2002. AVO and AVA inversion for fractured reservoir characterization. Geophysics. 67(1), 300–306.
DOI: https://doi.org/10.1190/1.1451802

[23] Ohaegbuchu, H.E., Igboekwe, M.U., 2016. Determination of subsurface rock properties from AVO analysis in Konga oil field of the Niger Delta, Southeastern Nigeria. Modeling Earth Systems and Environment. 2, 124.
DOI: https://doi.org/10.1007/s40808-016-0184-9

[24] Adeoti, L., Ikoro, C.O., Adesanya, O.Y., et al., 2019. On the effectiveness of using quantitative avo analysis in fluid and lithology discrimination in an offshore Niger Delta Field, Nigeria. Ife Journal of Science. 21(1), 1–12.
DOI: https://doi.org/10.4314/ijs.v21i1.1

[25] Nwokoma, E., Agbasi, O.E., Dinneya, O.C., 2022. Prediction of litho-porosity using incompressibility and rigidity, offshore Niger Delta, Nigeria. Geoinformatica Polonica. 21, 31–42.
DOI: https://doi.org/10.4467/21995923gp.22.003.17081

[26] Adeoti, L., Adeleye, K.O., Itsemode, A., et al., 2015. Fluid prediction using AVO analysis and forward modelling of deep reservoirs in Faith Field, Niger Delta, Nigeria. Arabian Journal of Geosciences. 8, 4057–4074.
DOI: https://doi.org/10.1007/s12517-014-1476-x

[27] Allo, O.J., Bako, M.E., Esan, D., 2022. Seismic attribute analysis for prospect delineation in 'TMB' field, Niger Delta Basin, Nigeria. Journal of Applied Sciences and Environmental Management. 26(3), 487–494.
DOI: https://doi.org/10.4314/jasem.v26i3.17

[28] Agbasi, O.E., Igboekwe, M.U., Chukwu, G.U., et al., 2018. Discrimination of pore fluid and lithology of a well in X Field, Niger Delta, Nigeria. Arabian Journal of Geosciences. 11, 274.
DOI: https://doi.org/10.1007/s12517-018-

3610-7

[29] Onyena, A.P., Sam, K., 2020. A review of the threat of oil exploitation to mangrove ecosystem: Insights from Niger Delta, Nigeria. Global Ecology and Conservation. 22, e00961.
DOI: https://doi.org/10.1016/j.gecco.2020.e00961

[30] Ogbe, O.B., 2020. Sequence stratigraphic controls on reservoir characterization and architectural analysis: A case study of Tovo field, coastal swamp depobelt, Niger Delta Basin, Nigeria. Marine and Petroleum Geology. 121, 104579.
DOI: https://doi.org/10.1016/j.marpetgeo.2020.104579

[31] Ogbe, O.B., 2021. Reservoir sandstone grain-size distributions: Implications for sequence stratigraphic and reservoir depositional modelling in Otovwe field, onshore Niger Delta Basin, Nigeria. Journal of Petroleum Science and Engineering. 203, 108639.
DOI: https://doi.org/10.1016/j.petrol.2021.108639

[32] Ugbor, C.C., Ugwuoke, C.I., Odong, P.O., 2023. Hydrocarbon prospectivity and risk assessment of "Bob" field central swamp depobelt, onshore Niger Delta Basin, Nigeria. Open Journal of Geology. 13(8), 847–882.
DOI: https://doi.org/10.4236/ojg.2023.138038

[33] Unukogbon, N.O., Asuen, G.O., Emofurieta, W.O., 2008. Sequence stratigraphic appraisal: Coastal swamp depobelt in the Niger Delta Basin Nigeria. Global Journal of Geological Sciences. 6(2), 129–137.
DOI: https://doi.org/10.4314/gjgs.v6i2.18762